A Combined Computational and Experimental Study of the Hydrogen-Bonded Dimers of Xanthine and Hypoxanthine

Thomas Hupp,[†] Christian Sturm,[†] Eline M. Basílio Janke,[‡] Montserrat Pérez Cabre,[‡] Klaus Weisz,*[,§] and Bernd Engels*[,†]

Institut für Organische Chemie, Universität Würzburg, Am Hubland, D-97070 Würzburg, Institut für Chemie, Freie Universität Berlin, Takustr. 3, D-14195 Berlin, and Institut für Chemie und Biochemie, Ernst-Moritz-Arndt-Universität Greifswald, Soldmannstr. 16, D-17487 Greifswald

Received: September 1, 2004; In Final Form: December 19, 2004

In addition to uracil, the noncanonical nucleobases xanthine and hypoxanthine are important lesions that are formed from the canonical bases when a cell is under oxidative stress. It is known that they lead to point mutations; however, more detailed information about their ability to form hydrogen-bonded complexes is not available. In the present paper such information is obtained by a combined experimental and theoretical approach. Accurate association constants of xanthosine and inosine dimers are determined by concentration dependent ^{1}H NMR experiments, and a structural characterization of individual complexes formed in solution is performed through measurements under slow exchange conditions at very low temperatures. An interpretation of the experimental data concerning complex geometries becomes possible through a comparison of measured and computed NMR chemical shifts. Further qualitative insights into the hydrogen bonding abilities of xanthine and hypoxanthine are obtained by a theoretical characterization of all possible pairing modes of xanthine and hypoxanthine dimers and by a comparison with simplified model systems. The influence of a polar medium on the bonding properties is also estimated and the importance of the various effects is discussed. Our analysis shows to what extent secondary electronic and electrostatic effects influence the hydrogen bonding properties of xanthine and hypoxanthine in the gas phase and in polar solvents.

Introduction

Next to uracil, the noncanonical nucleobases xanthine **1** and hypoxanthine **2** (Figure 1) are important lesions that are formed from the canonical bases when a cell is under oxidative stress.[1] Thus, both are found in epidermal skin or calf thymus after exposure to cigarette smoke.[2] They originate from the canonical bases guanine[3] and adenine by nitrogen loss, which occurs either spontaneously by hydrolysis or at a much higher rate due to reactions with free radicals such as OH and NO[4,5] or nitrous acid.[6,7] The formation of xanthine and hypoxanthine leads to point mutations,[8] which indicates that both are able to form Watson−Crick base pairs with the canonical pyrimidine bases thymine and cytosine, respectively. While the existence of such base pairs is proven, structural and/or stability information is not available.[8,9] Studies about tautomeric forms of xanthine and hypoxanthine were already performed.[10]

The stability of the individual hydrogen bonds in the complexes correlates with the acidity of the hydrogen bond donors, i.e., the polarization of the hydrogen atoms and the basicity of the hydrogen bond acceptors.[11] However, since both systems possess several acceptor and donor units, cooperative effects such as interactions with neighboring H-bond donor and acceptor functionalities also influence considerably the stability of the hydrogen-bonded systems. Such effects are termed secondary electrostatic interactions.[12] A well-known example

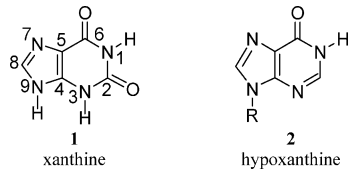

Figure 1. Xanthine **1** and hypoxanthine **2**. The enumeration indicated for xanthine is also used for hypoxanthine.

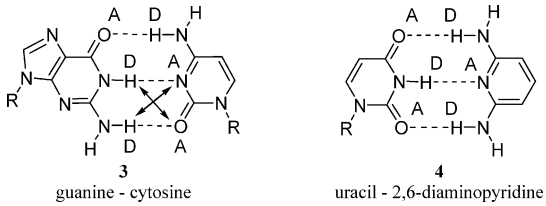

Figure 2. Canonical Watson−Crick base pairs between guanine and cytosine **3** and uracil and 2,6-diaminopyridine **4**.

given by Jorgensen and Pranata[12] that indicates the importance of such effects is the strong binding in the guanine−cytosine Watson−Crick base-pair **3** shown in Figure 2. It is more than twice as strong compared to the base pair between uracil and 2,6-diaminopyridine **4**, even though both pairings have the same number of hydrogen bonds. However, while the importance of secondary effects is generally accepted, it has been questioned whether they are sufficient to fully explain the stability of the hydrogen-bonded complexes.[13] Another secondary effect was proposed by Gilli.[14] It leads to a stabilization of hydrogen bonds due to the polarization of the π-electron system.

The importance of secondary electrostatic interactions for the relative stabilities of the various pairing modes of hydrogen-

* Corresponding authors. (experiment) E-mail: weisz@uni-greifswald.de. (theory) E-mail: bernd@chemie.uni-wuerzburg.de

[†] Universität Würzburg.

[‡] Freie Universität Berlin.

[§] Ernst-Moritz-Arndt-Universität Greifswald.

10.1021/jp0460588 CCC: $30.25
Published on Web 02/08/2005

bonded dimers of xanthine **1** is due to the fact that all two-dentate pairing modes are formed by the same functional groups. Consequently, the differences in their stability can result only from effects induced by functional groups not directly involved in the base pairing. In addition to such effects, those discussed by Gilli[14] are also expected to be important for the stability differences of self-pairing complexes of xanthine and of hypoxanthine. Therefore, a comparison of the various pairs can broaden the knowledge about cooperative effects in hydrogen bond networks. Taking solvent effects into account, it can be estimated how a polar solvent can change the relative importance of the different effects.

To characterize the hydrogen bonding properties of xanthine and hypoxanthine in the present paper, the dimers of xanthosine and inosine (the ribosylated derivatives of xanthine and hypoxanthine) are characterized by NMR spectroscopy, while computations are used to describe the properties of the unsubstituted noncanonical bases. The stabilities of xanthosine and inosine dimers are determined by concentration dependent ^{1}H NMR experiments which allow the determination of accurate association constants. Through measurements under slow exchange conditions at very low temperatures a structural characterization of individual complexes formed in solution is performed. An interpretation of the experimental data is obtained through the computation of the NMR chemical shifts of all possible pairing modes of xanthine and hypoxanthine.

Further insight into the hydrogen bonding abilities of xanthine and hypoxanthine is obtained by a theoretical characterization of all possible pairing modes of xanthine and hypoxanthine dimers. The influence of a polar medium on the bonding properties is also estimated. These calculations enable a more general picture of the abilities of xanthine and hypoxanthine to form hydrogen-bonded complexes. Through a comparison with simplified model systems it is investigated what kind of secondary effects influence these abilities in the gas phase and in polar solvents.

Methods

Experimental Methods. NMR experiments were performed on a Bruker AMX500 spectrometer. Temperatures were adjusted by a Eurotherm variable temperature unit to an accuracy of ±1.0 °C. Temperature calibration was performed with a sample of methanol in MeOH-d_4 and the calibration curve extrapolated for temperatures outside the range covered by the methanol sample. ^{1}H chemical shifts in methylene chloride at 293 K were referenced relative to $CHDCl_2$ (δ_H = 5.32 ppm) and in a Freon mixture relative to $CHClF_2$ (δ_H = 7.13 ppm). Concentration dependent chemical shifts were fitted with an appropriate equation by employing the Marquardt−Levenberg algorithm.

Materials. The deuterated Freon mixture $CDClF_2/CDF_3$ was prepared as described elsewhere[15] and handled on a vacuum line which was also used for the sample preparation. Protection of the sugar OH groups was achieved by O-silylation[16,17] of the xanthine and hypoxanthine nucleosides. All reactions were controlled by TLC on silica gel plates (Merck silica gel 60 F_{254}). When necessary, solvents were dried by standard procedures prior to use.

2′,3′,5′-Tri-O-(tert-butyldimethylsilyl)-Xanthosine. To a solution of 0.57 g of xanthosine (2 mmol) and 4.36 g of imidazole (64 mmol) in 5 mL of dry DMF was added 4.82 g of *tert*-butyldimethylsilyl chloride (32 mmol). The gel-like solution was stirred for 2 days at room temperature under an argon atmosphere while the reaction was followed by TLC on silica gel plates (CH_2Cl_2/CH_3OH 10:0.5). After the addition of 60 mL of 1 M aqueous sodium hydrogen carbonate, the aqueous phase was extracted with 200 mL portions of dichloromethane. The pooled organic phase was dried over sodium hydrogen carbonate, filtered and concentrated by rotary evaporation. Remaining DMF solvent was evaporated at 100 °C at low pressure to give a liquid product, which was subsequently dissolved in CH_2Cl_2 and purified by column chromatography (silica gel, CH_2Cl_2/CH_3OH 10:0.3). Final purification by HPLC provided 0.79 g (1.26 mmol, 63%) of pure 2′,3′,5′-tri-*O*-(*tert*-butyldimethylsilyl)-xanthosine. ^{1}H NMR (250 MHz, CD_2Cl_2): δ (ppm) −0.35 (s, 3H, CH_3Si), −0.03 (s, 3H, CH_3Si), 0.12 (s, 3H, CH_3Si), 0.14 (s, 3H, CH_3Si), 0.23 (s, 3H, CH_3Si), 0.28 (s, 3H, CH_3Si), 0.83 (s, 9H, $(CH_3)_3C$), 0.94 (s, 9H, $(CH_3)_3C$), 1.01 (s, 9H, $(CH_3)_3C$), 3.91 (dd, 1H, H5′), 4.06 (dd, 1H, H5″), 4.13 (m, 1H, H4′), 4.16 (m, 1H, H3′), 4.19 (m, 1H, H2′), 5.67 (d, 1H, H1′), 7.44 (s, 1H, H8), 8.71 (s, 1H, N1−H), 9.65 (s, 1H, N3−H).

2′,3′,5′-Tri-O-(tert-butyldimethylsilyl)-Inosine. 2.68 g (10 mmol) of inosine and 4.09 g (60 mmol) of imidazole were dissolved in 60 mL of dry DMF. After the addition of 5.32 g (35.29 mmol) of *tert*-butyldimethylsilyl chloride, the mixture was stirred for 2 days at room temperature under an argon atmosphere while the reaction was followed by TLC on silica gel plates (CH_2Cl_2/CH_3OH 10:0.5). After adding 30 mL of a 1 M aqueous solution of sodium hydrogen carbonate, the aqueous phase was extracted with 200 mL portions of dichloromethane. The combined extracts were concentrated at reduced pressure and purified by column chromatography (silica gel, CH_2Cl_2/CH_3OH 10:0.3). Even after repeated recrystallizations from methanol−water, only a mixture of di- and trisilylated product was obtained. However, final purification with reversed phase HPLC (CH_2Cl_2:CH_3OH 10:0.2) afforded 2.5 g (4.09 mmol, 41%) of pure 2′,3′,5′-tri-*O*-(*tert*-butyldimethylsilyl)-inosine. ^{1}H NMR (250 MHz, CD_2Cl_2) δ (ppm): −0.17 (s, 3H, CH_3Si), −0.07 (s, 3H, CH_3Si), 0.11 (s, 3H, CH_3Si), 0.12 (s, 3H, CH_3Si), 0.15 (s, 3H, CH_3Si), 0.16 (s, 3H, CH_3Si), 0.81 (s, 9H, $(CH_3)_3C$), 0.94 (s, 9H, $(CH_3)_3C$), 0.97 (s, 9H, $(CH_3)_3C$), 3.98 (dd, 1H, H5′), 4.01 (dd, 1H, H5″), 4.14 (m, 1H, H4′), 4.32 (t, 1H, H3′), 4.53 (t, 1H, H2′), 6.02 (d, 1H, H1′), 8.22 (s, 1H, H2), 8.24 (s, 1H, H8), 12.89 (s, 1H, N1−H).

Computational Details. All dimerization energies given were computed with the MP2 approach in the RI-approximation and the B3LYP-functional,[18] both in combination with the TZVPP basis set.[19] The basis set superposition error (BSSE) was corrected according to the Boys−Bernardi counterpoise procedure.[20] All calculations were performed with the TURBOMOLE[21] or the GAUSSIAN program.[22] The geometries for the dimers and monomers of N9-xanthine were computed using the B3LYP functional in combination with the 6-31++G(d,p) basis set.[23] These geometry optimizations were performed with the Gaussian98 program package. All other structures were optimized with the BLYP functional in the TZVP[24] basis set which, due to the RI[25] approximation used, allowed a much faster optimization of the hydrogen-bonded dimers than the B3LYP/6-31++G(d,p) ansatz. Bond lengths obtained by the B3LYP/6-31++G(d,p) and the BLYP/TZVP approaches differ by less than 0.01 Å for regular and by less than 0.03 Å for hydrogen bonds. Geometry optimizations employing the MP2 method also gave very similar results (see Supporting Information). The geometrical data given in Figure 10 are always taken from BLYP/TZVP optimizations. All minima were checked by frequency calculations. Test calculations in which geometries were optimized within a polar solvent show no differences. Consequently, the gas-phase geometries were employed for the solvent computations.

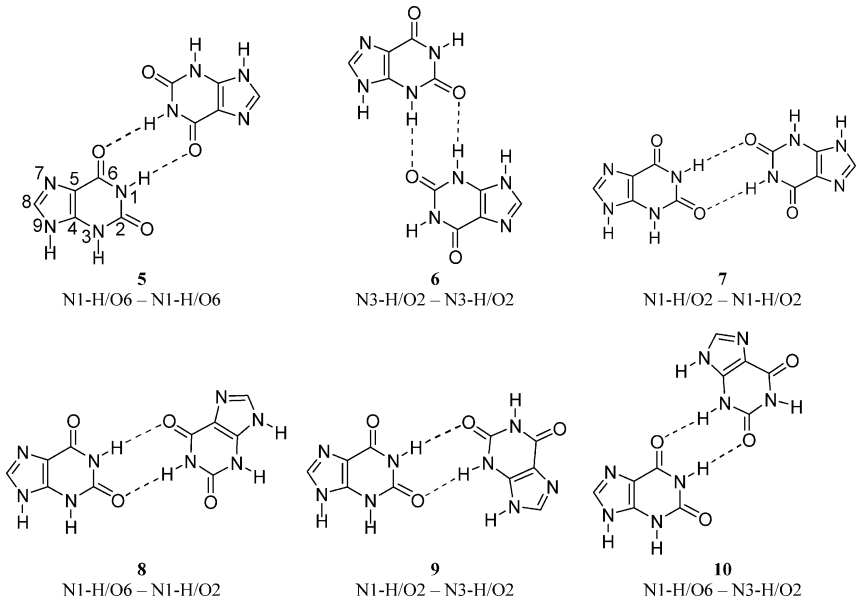

Figure 3. Possible hydrogen-bonded base pairs of N9-xanthine.

In most computations the influence of a solvent is dissected in several parts.[26] In the present paper the so-called electrostatic contributions (often also abbreviated as electrostatic component of solvation) were estimated using the COSMO[27] approach as implemented in TURBOMOLE[27b] with a dielectric constant of $\epsilon = 40$ to simulate the Freon solvent. For some model systems the value of $\epsilon = 78$ is used to give an upper limit for a dipolar solvent. However, differences between the results obtained with $\epsilon = 40$ and those with $\epsilon = 78$ are very small (0.1−0.4 kcal/mol). Nonelectrostatic effects of the solvent were estimated employing the GAUSSIAN98 program. Since Freon is not parametrized, the parametrization for acetonitrile was used. Acetonitrile possesses the most similar surface tension and dielectric constant to the Freon mixture used in the experiments. To ensure that this approximation does not lead to significant errors we also performed computations employing the parametrization of nitromethane and water. The computed values differ by less than 1 kcal/mol. The corrections for the various complexes differ by less than 0.1 kcal/mol, i.e., these effects are less important for the understanding of differences between the various complexes.

Thermodynamic corrections for the gas phase were obtained using the standard implementation of the TURBOMOLE program package. Gas phase corrections are often also employed for estimating the correction for polar solvents. However, since we found that the corrections correlated with the strength of the hydrogen bonds, we recomputed the corrections employing the COSMO approach. While this approach estimates the influence of a polar solvent connected with vibrational effects, e.g., on S_{vibr}, the standard gas-phase values are employed for S_{trans}. For a better estimate we used an approach introduced by Williams and co-workers.[28] In this approach the change in entropy when going from a gas to a 1 M solution is broken down into two hypothetical stages: the gas is first condensed into a liquid, and this "pure" liquid is finally diluted to a concentration of 1 M. More information can be taken from the literature.[28]

^{1}H NMR-spectra were computed using the HF approach in combination with the TZVP basis set using the gauge including atomic orbital method.[29] The HF is used since it was found to give quite reliable ^{1}H NMR chemical shifts.[30]

Descriptions of the ^{1}H NMR Experiments. Figure 3 shows the six possible two-dentate dimerization modes **5**−**10** of diketo xanthine. The numbering of the atomic centers of xanthine can be taken from pairing mode **5**. To determine the most stable pairing mode and its equilibrium constant for xanthine self-association we measured ^{1}H chemical shifts for the imino protons of the *O*-protected nucleosides as a function of concentration. The employment of the tri-*O*-*tert*-butyldimethylsilyl protected ribonucleosides strongly enhances nucleoside solubility in apolar solvents and enables measurements with concentrations of up to 100 mM. Isotherms for the inosine and xanthosine nucleosides in CD_2Cl_2 at 296 K are shown in Figure 4. H1 and H3 xanthosine protons were unambiguously assigned based on their nuclear Overhauser effect (NOE) connectivities (vide infra). Most noticeably, the more deshielded xanthosine H3 imino resonance exhibits no concentration-dependent chemical shift excluding its participation in an intermolecular hydrogen bond. In contrast, the xanthine H1 imino signal experiences a downfield shift with increasing nucleoside concentration; however, the shifts are clearly less pronounced compared to the inosine H1 proton resonance. A nonlinear least-squares fit of

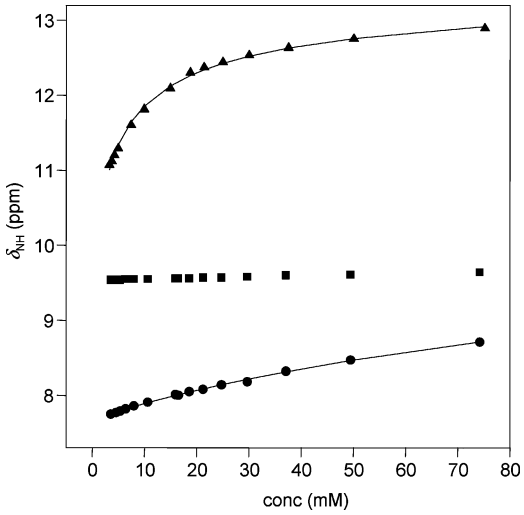

Figure 4. Concentration dependent H1 (circles) and H3 (squares) imino proton chemical shift of 2′,3′,5′-tri-*O*-(*tert*-butyldimethylsilyl)-xanthosine and H1 (triangles) imino proton chemical shift of 2′,3′,5′-tri-*O*-(*tert*-butyldimethylsilyl)-inosine in CD_2Cl_2 at 296 K. Lines represent the least-squares fit.

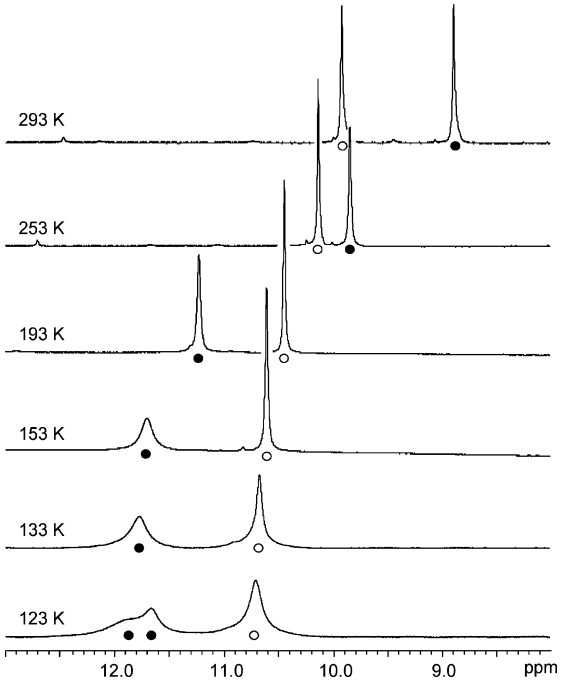

Figure 5. Temperature dependent ^{1}H NMR spectra showing the NH proton spectral region of 2′,3′,5′-tri-*O*-(*tert*-butyldimethylsilyl)-xanthosine in Freon. Filled and open circles denote H1 and H3 imino proton signals, respectively.

the H1 chemical shifts to a fast monomer−dimer equilibrium yields association constants of 200 ± 10 M^{-1} for inosine and 2.5 ± 0.3 M^{-1} for xanthosine. In addition to its larger association constant, the limiting chemical shift of the imino H1 proton in inosine at infinite concentration as determined by the fitting procedure amounts to 13.7 ppm and is thus at lower field compared to the xanthosine H1 proton with a limiting chemical shift of 12.3 ppm.

Data obtained from ^{1}H chemical shift measurements at ambient temperatures only represent averages over all coexisting species and do not allow a detailed evaluation of the type and relative population of the self-associates present in solution. To study the preferred association modes of xanthosine and inosine in more detail, we performed NMR measurements at temperatures low enough for any coexisting dimers to be in slow exchange. For this purpose, a deuterated Freon mixture $CDClF_2$/CDF_3 was used as solvent allowing measurements in the liquid state down to 100 K.[31a−e]

^{1}H NMR spectra showing the imino proton resonances of silylated xanthosine in Freon are plotted as a function of temperature in Figure 5. A gradual downfield shift of the imino proton signals with decreasing temperature can be attributed to an increased formation of hydrogen-bonded dimers. However, a much larger temperature dependence of the H1 chemical shift results in a more deshielded H1 proton at low temperatures. Below 133 K this resonance splits into two separate signals with chemical shifts of 11.88 and 11.68 ppm. Clearly, such a situation indicates different coexisting dimeric species being in slow exchange. In contrast, only one resolved signal at 10.69 ppm is observed for the H3 imino proton, even at very low temperatures.

To establish the nucleoside conformation and the geometry of formed dimers, a 2D NOE experiment of xanthosine was acquired at 125 K (not shown). The H8 base proton exhibits a strong connectivity to the anomeric H1′ proton but lacks additional cross-peaks to other sugar protons. At the same time, strong NOE cross-peaks connect the imino resonance at 10.69 ppm with H2′, H3′, and the 5′-TBDMS methyl protons. The two downfield shifted imino signals at 11.68 and 11.88 ppm are not connected to any other protons by observable NOE contacts. Because the xanthosine nucleoside evidently adopts a syn glycosidic torsion angle with the purine ring system located above the sugar ring,[32] the H3 proton is unambiguously assigned to the imino signal at 10.69 ppm and the isolated H1 proton to the two downfield shifted imino resonances. As shown in Figure 6 such a conformation allows the formation of an intramolecular hydrogen bond between H3 and the O5′ oxygen of the sugar. Clearly, this intramolecular hydrogen bond not only accounts for the downfield shifted H3 resonance at room temperature, but also for the small concentration and temperature dependence of the H3 imino proton chemical shift.

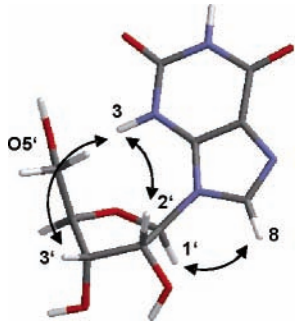

Figure 6. Molecular model of xanthosine with a syn glycosidic torsion angle. Arrows indicate strong NOE cross peaks observed experimentally.

With the 3-imino group of xanthosine engaged in an intramolecular hydrogen bond, only the cyclic dimers **5**, **7**, and **8** (see Figure 3) may be formed in solution. Unfortunately, assignment to a particular geometry is hampered by the lack of protons in close proximity to the hydrogen-bonded H1 imino proton in the various self-associates preventing the observation of diagnostic ^{1}H-^{1}H NOE contacts at low temperatures. However, the presence of at least two resolved H1 protons of approximately equal intensity is only compatible with the formation of the asymmetric dimer **8** and/or a mixture of the symmetric dimers **5** and **7**.

We also recorded ^{13}C NMR spectra of xanthosine in a chloroform solution at ambient temperatures to follow the chemical shift of the C2- and C6-carbonyl carbon as a function of concentration (spectra not shown). Upon 4-fold dilution, both carbonyl carbon resonances undergo a moderate upfield shift as expected for the loss of hydrogen bond interactions at both sites. However, because the two carbonyl groups are likely to be differently affected upon participating in a hydrogen bond, the relatively small shift differences observed for ^{13}C2 (0.34 ppm) and ^{13}C6 (0.23 ppm) prohibit a more quantitative analysis in terms of the predominant acceptor site without knowledge of the individual perturbation in their electron distribution.

The temperature dependence of the inosine imino proton resonance in Freon is shown in Figure 7. Again, upon cooling the imino proton signal experiences a downfield shift due to increased self-association. Also the imino resonance broadens at low temperatures as expected for a slower molecular reorientation but there is no indication of signal splitting in the temperature range studied. At 123 K the chemical shift of the imino proton has reached its limiting value at 13.87 ppm and does not change on further lowering the temperature. Disregarding complete signal overlap, the observation of a single resonance at low temperatures indicates the existence of only one dimer type in solution. Also, using the proton chemical shift as indicator for the relative strength of hydrogen bonds, the

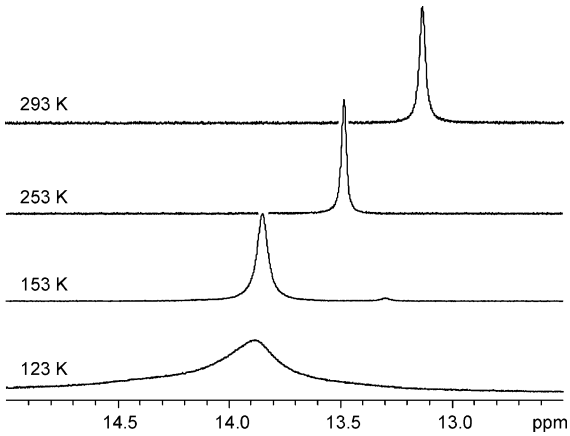

Figure 7. Temperature dependent ^{1}H NMR spectra showing the NH proton spectral region of 2′,3′,5′-tri-*O*-(*tert*-butyldimethylsilyl)-inosine in Freon.

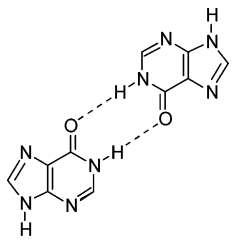

11

Figure 8. Symmetric homodimer of hypoxanthine.

observation of a more deshielded inosine imino proton compared to xanthosine imino protons in the dimers indicates its participation in a stronger and shorter hydrogen bond.[33]

We also performed a 2D NOE experiment on inosine at 123 K. Since at intermediate temperatures a resolved H2 doublet is observed due to the scalar coupling with the vicinal imino proton (^3J = 3.7 Hz), H8 and H2 protons can be unambiguously identified. Intramolecular NOE contacts between sugar protons and H8 but not H2 clearly establish an anti orientation for this nucleoside with a glycosidic torsion angle in the 180° range at low temperatures. Except for a strong intrabase cross-peak with H2, the H1 imino resonance exhibits no other internucleoside cross-peaks as expected for a symmetric homodimer **11** with two cyclic hydrogen bonds between H1 and the O6 carbonyl oxygen (Figure 8).

Computations

Based on the NMR experiments alone, an unequivocal determination of the pairing geometry for the xanthine dimers is not possible. However, the computed stabilities or NMR chemical shifts of the various pairing modes may be used for an assignment if the differences between the various pairing modes in either stability or NMR chemical shifts are larger than the error bars of the method of calculation. Consequently, the stabilities of the pairing modes must differ by at least 1−2 kcal/mol to unambiguously interpret the experimental data. However, in addition to an assignment of the experiment, an analysis of the energetics of the formation process also allows the characterization of those pairing modes that are not accessible by the experiment (e.g., **6**, **9**, and **10**). Such computations also enable an insight into the interplay of the various effects such as electronic and electrostatic secondary effects, the influence of a polar solvent, or the influence of the entropy, which are all expected to influence the stability of the dimers.

TABLE 1: Energetic Characterization of Xanthine Dimers (gas phase) at T = 128 K (all values in kcal mol^{-1}, except for ΔS, which is given in cal mol^{-1} K^{-1})

	$^a\Delta E_{\text{MP2/TZVPP}}$	$^b\Delta E_{\text{B3LYP/TZVPP}}$	$^c\Delta E \rightarrow \Delta H$	$^d\Delta H$	$^e\Delta E \rightarrow \Delta G$	$^d\Delta G$
5	−10.9	−9.6	+0.8	−8.8	+6.1	−3.5
6	−22.0	−20.2	+1.4	−18.8	+7.2	−13.0
7	−10.6	−8.8	+0.7	−8.1	+6.0	−2.8
8	−10.5	−8.8	+1.2	−7.6	+6.8	−2.0
9	−14.8	−13.0	+1.2	−11.8	+6.7	−6.3
10	−17.1	−15.7	+0.9	−14.8	+6.3	−9.4

[a] Dimerization energies were obtained from MP2/TZVPP computations in the gas phase. Counterpoise corrections were applied. [b] Dimerization energies were obtained from B3LYP/TZVPP computations in the gas phase. Counterpoise corrections were applied. [c] Thermodynamic corrections for enthalpy within the gas phase (B3LYP/TZVPP computations). They were obtained with the SNF program of the TURBOMOLE suite. [d] Based on B3LYP/TZVPP. [e] Thermodynamic corrections for the free energy computed for the gas phase (B3LYP/TZVPP computations). They were obtained with the SNF program of the TURBOMOLE suite.

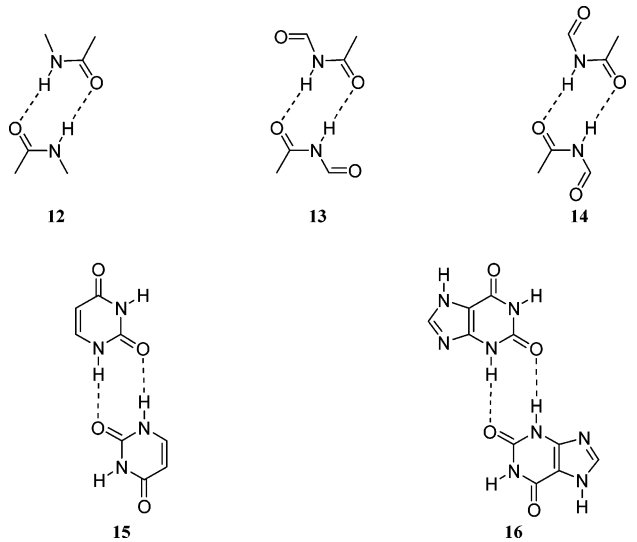

12 **13** **14** **15** **16**

Figure 9. Hydrogen-bonded dimers of *N*-methylacetamide **12**, cis *N*-formylacetamide **13**, and trans *N*-formylacetamide **14**, uracil **15** and N7-xanthine **16** forming hydrogen bonds with the N3−H donor functionality.

Table 1 summarizes the stabilities of pairing modes **5**−**10** in the gas phase. Although all cases represent two-dentate pairing modes, the dimerization energies (ΔE) for the gas phase range from −10 to −22 kcal/mol (MP2). Those of the reverse Watson−Crick pairs **5** and **7** and Watson−Crick pair **8** (−10.9, −10.6, and −10.5 kcal/mol, respectively) lie in the lower range of the stabilization energies known for two-dentate base pairs, the dimerization energy of the strongest bonded base pair **6** is twice as large (ΔE = −22.0 kcal/mol in the MP2/TZVPP approach). Please note, that for predictions of the relative stabilities both theoretical approaches already differ by 1−2 kcal/mol.[34]

To investigate whether the variation in the dimerization energies is connected with either the electronic nature of the hydrogen bond donor unit or with different secondary electrostatic effects, pairing modes **5** and **6**, in which either only the N1−H or only the N3−H unit is involved as hydrogen bond donor, were analyzed in greater detail. Possible secondary effects in the pairing of **5** can be studied with the simple model systems **12**−**14** illustrated in Figure 9. Figure 9 also shows uracil **15** and a pairing mode of the N^7 regioisomer **16** allowing further insight into the secondary interactions of **6**. In these systems

TABLE 2: Gas Phase Dimerization Energies of the Amide Dimers 12−16 (all values in kcal mol^{-1})

		MP2/TZVPP	B3LYP/TZVPP
12	*N*-methylacetamide	−14.4	−13.1
13	cis *N*-formylacetamide	−9.2	−7.9
14	trans *N*-formylacetamide	−13.1	−12.2
15	uracil	−17.2	−16.0
16	N7-xanthine	−14.1	−12.5

only the secondary effects vary while the electronic character of the nitrogen centers are very similar to **5**.

The dimerization energies of **12**−**16** are given in Table 2. The simple *N*-methylacetamide **12** has a dimerization energy of −14.4 kcal/mol. The cis-configurated *N*-formylacetamide **13** has a considerably lower dimerization energy of −9.2 kcal/mol while its *trans*-isomer **14** has a dimerization energy of −13.1 kcal/mol which is only 1.3 kcal/mol lower than the value computed for **12**. The dimerization energies are grouped around the value of the pairing mode **5** of dixanthine. **13** and **14** mainly differ by the relative position of the carbonyl groups that do not participate in hydrogen bonding. For **13**, these groups are only 3.94 Å apart from the carbonyl group of the second unit which is involved in the hydrogen bond, so that an electrostatic repulsion between the partially negatively charged moieties can be expected. For **14**, due to the *trans*-configuration, the repulsive interaction is diminished. Since the electronic character of the nitrogen centers of both compounds should be very similar, the repulsive interaction seems to be the major reason for the difference in the dimerization energies of **13** and **14**.

The presence of very similar repulsive secondary electrostatic effects in pairing mode **5** of xanthine and in **13** is also supported by a comparison of the geometries for both systems (Figure 10). In both systems, the NH−O-angle deviates by 8−9° from the idealized H-bond angle of 180°. Furthermore, the hydrogen bond lengths (b in Figure 10) and the distance between the participating H-bonded and the spectator oxygen atom (a in Figure 10) of both systems agree within 0.1 Å. Please note that **5**, in line with its lower dimerization energy (−10.9 vs −9.2 kcal/mol for **13** on the MP2 level) possesses somewhat shorter hydrogen bonds. It is obvious that this difference cannot be explained by different secondary interactions, but, as it will be explained for hypoxanthine, should result from interactions related to the polarization of the π-electron system.

Insight into the factors leading to the unusually high stability of pairing mode **6** of dixanthine can be obtained by a comparison between **6** (Figure 3) and the corresponding pairing modes of uracil **15** and of the regioisomer N7-xanthine **16** as shown in Figure 9. The corresponding dimerization energies obtained in the gas phase are also summarized in Table 2. The geometric parameters of the H-bonds are shown in Figure 10. Going from uracil **15** to the xanthine complexes **6** or **16** one either places a partially positively charged hydrogen atom of an NH-unit or a partially negatively charged nitrogen center next to the N3−H groups participating in the hydrogen bonds (for simplicity, the same atom numbering as indicated in Figure 3 for xanthine is used for uracil). In line with the arguments given for the series **12**−**14**, the partially negatively charged nitrogen centers in **16** should repel the oxygen centers of the carbonyl groups which are involved in the hydrogen bond. Indeed, Table 2 shows a decrease in the dimerization energy of about 3.1 kcal/mol (MP2/TZVPP) if one goes from **15** to **16**. The effect is smaller than the effect found between **12** and **13**, which is reasonable since the distance between the carbonyl oxygen and the nitrogen center is 4.15 Å (bond a of **16** in Figure 10), while the corresponding distance in **13** is 3.94 Å (bond a of **13** in Figure 10). Going from **15** to **6**, a partially positively charged hydrogen center of an NH unit is positioned beside the NH group which forms the hydrogen bond. For **6** the hydrogen center has a distance of about 3.50 Å (bond a of **6** in Figure 10) from the carbonyl group which participates in the hydrogen bond. The attraction between both centers stabilizes the hydrogen bond and indeed the absolute value of the dimerization energy of **6** is about 4.8 kcal/mol higher than that of its counterpart **15**.

The thermodynamic corrections leading from dimerization energies to dimerization enthalpies ($\Delta E \rightarrow \Delta H$) or to dimerization free energies ($\Delta E \rightarrow \Delta G$) of the various xanthine dimers are quite large (0.7−1.4 kcal/mol and 6.0−7.2 kcal/mol, respectively). Although the corrections are considerably more uniform than the dimerization energies, a correlation between the size of the

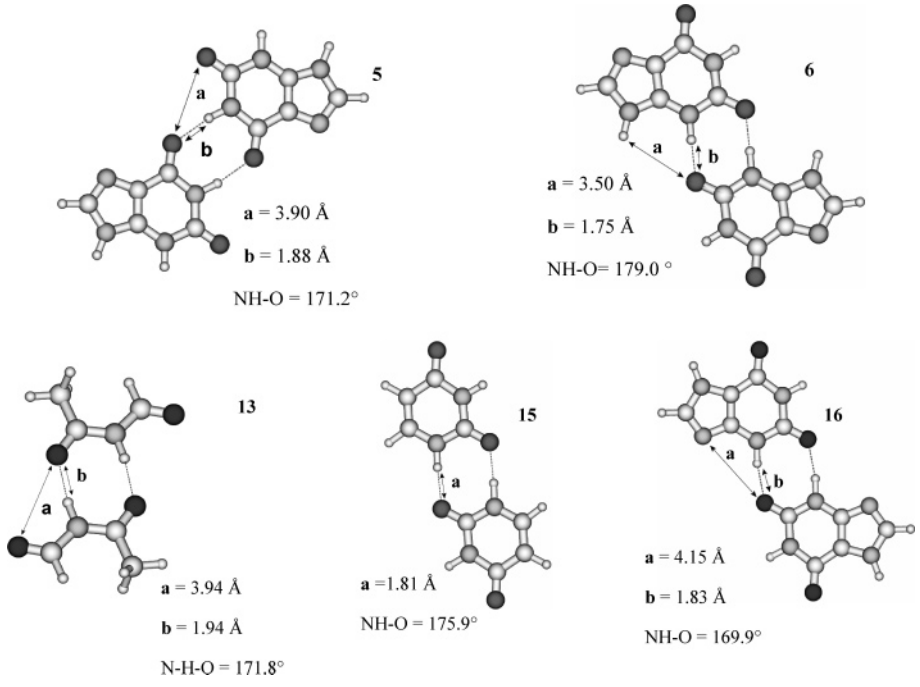

Figure 10. Hydrogen bond lengths, angles, and distances between carbonyl groups of **5**, **6**, **13**, **15,** and **16**.

TABLE 3: Estimated Dimerization Enthalpies for Xanthine Dimers in Freon ($\epsilon = 40$) at $T = 128$ K (all values in kcal mol^{-1})

	[a]ΔE	[b]n.e.	ΔE+n.e.	[c]ΔH (gas)	[d]$\Delta E \rightarrow \Delta H$ (ϵ=40)	[d]ΔH (ϵ=40)
5	−3.4	−1.5	−4.9	−4.1	+0.8	−4.1
6	−4.8	−1.5	−6.3	−4.9	+0.8	−5.5
7	−2.9	−1.5	−4.4	−3.7	+0.9	−3.5
8	−3.0	−1.5	−4.5	−3.3	+0.8	−3.7
9	−3.9	−1.5	−5.4	−4.2	+0.9	−4.5
10	−4.5	−1.5	−6.0	−5.1	+0.7	−5.3

[a] Dimerization energies obtained in a polarizable medium with ϵ=40 (COSMO) employing the B3LYP functional in combination with a TZVPP basis set. Counterpoise corrections were applied. [b] Nonelectrostatic interactions (free energy of cavity, dispersion-repulsion interaction between solute and solvent). Since Freon is not parametrized, the parametrization of acetonitrile was used. The calculations were performed with GAUSSIAN98. [c] The thermodynamic corrections for enthalpies were taken from gas phase calculations. The respective values of the thermodynamic corrections are given in Table 1 column 4. [d] Thermodynamic corrections were taken from calculations in which the influence of a polar medium is taken into account via the COSMO model ($\epsilon = 40$). The computations were performed with the SNF program of the TURBOMOLE suite.

TABLE 4: Estimated Dimerization Free Energies for Xanthine Dimers in Freon ($\epsilon = 40$) at $T = 128$ K (all values in kcal mol^{-1}. except for ΔS, which is given in cal mol^{-1} K^{-1}

	[a]ΔG (gas)	[b]ΔS_{rot} (ϵ=40)	[b]ΔS_{vibr} (ϵ=40)	[b,c]ΔS (ϵ=40)	[d]ΔS_{cor} (ϵ=40)	[d]$\Delta E \rightarrow \Delta G$ (ϵ=40)	[d]ΔG (ϵ=40)
5	+1.2	−22,12	15,11	−41.7	−24,14	+3.9	−1.0
6	+0.9	−22,14	14,12	−42.7	−25,15	+4.0	−2.3
7	+1.6	−22,21	15,38	−41.5	−23,96	+4.0	−0.4
8	+2.3	−22,12	15,31	−41.5	−23,93	+3.9	−0.6
9	+1.3	−22,15	14,78	−42.0	−24,50	+4.0	−1.5
10	+0.3	−22,10	11,67	−45.1	−27,56	+4.2	−1.8

[a] Based on the ΔE values from Table 3 column 2 and the corresponding nonelectrostatic contributions (Table 3, column 3). The thermodynamic corrections for Gibbs free energies were taken from gas-phase calculations (Table 1, column 6). [b] Thermodynamic corrections taken from calculations in which the influence of a polar medium is taken into account via the COSMO model (ϵ=40). The computations were performed with the TURBOMOLE-Suite. [c] In addition to ΔS_{rot} and ΔS_{vibr}, ΔS contains the contribution of ΔS_{trans} (−34,68 cal mol^{-1} K^{-1} for all pairing modes) obtained from the equations for the gas phase. This is the standard approach in most programs. [d] In addition to ΔS_{rot} and ΔS_{vibr} obtained from the COSMO computations, ΔS_{cor} contains the contribution of ΔS_{trans} obtained from the approach by Williams and co-workers.[28] For the xanthine dimers a value of $\Delta S_{trans} = -17.13$ cal mol^{-1} K^{-1} is obtained for all pairing modes. For more information see text.

TABLE 5: Comparison of the Dimerization Energies of the Various Model Systems Obtained with the COSMO Approach ($\epsilon = 78$, water)[a]

	5	**6**	**11**	**12**	**13**	**15**	**16**
B3LYP/TZVPP	−3.3	−4.4	−3.6	−1.9	−2.8	−4.4	−4.4

[a] All computations were performed with the B3LYP/TZVPP approach. All values in kcal mol^{-1}.

dimerization energies and the thermodynamic corrections exists. While for pairing mode **6** the corrections leading to the dimerization free energy ΔG are 7.2 kcal/mol, the weaker pairing modes **5**, **7**, and **8** possess corrections of about 6.0 kcal/mol.

Gas phase computations predict that the stabilities of the experimentally accessible pairing modes **5**, **7**, and **8** are very similar. Pairing mode **5** is computed to be the most stable ($\Delta G = -3.5$ kcal/mol), but **7** and **8** are predicted to be only 0.7 and 1.5 kcal/mol (B3LYP/TZVPP) less stable, respectively. If the MP2 approach is used, differences are even smaller. Due to such small differences, gas phase calculations are not sufficient for an unequivocal interpretation of the experiments in Freon matrices, since solvent effects are known to be crucial for the energetics of dimerization. Computations, which estimate the influence of a solvent on the basis of continuum approaches, are summarized in Table 3 (for the dimerization enthalpies) and Table 4 (for the dimerization free energies).

Generally, the solvation energy is dissected into several contributions. Important effects arise from the so-called electrostatic contributions,[26] which in the present work are estimated by employing the COSMO approach with $\epsilon = 40$ to model the influence of a Freon matrix at 128 K. Their influences are included in the dimerization energies (ΔE) given in Table 3. The absolute values of these dimerization energies are smaller by a factor of 3 or 4 compared to the values obtained in the gas phase (Table 1, column 2). The relative order of the various pairing modes remains, but the differences of up to 12 kcal/mol in the gas phase shrink to only 1.8 kcal/mol. A similar trend is found for all model systems (Table 5). The strong decrease of the differences within a polar solvent supports our conclusion that long range electrostatic interactions are mainly responsible for the differences in the dimerization energies of the investigated systems. For a polar solvent, the computed differences between the pairing modes **5**, **7**, and **8** are only around 0.5 kcal/mol.

The second contribution to the solvation energy includes the energies necessary to form the cavity for the solute and the dispersion−repulsion forces between solute and solvent molecules. They are often summarized as nonelectrostatic contributions (abbreviated as n.e. in Table 3).[26] Since for Freon no parameters exist, we used the most appropriate parametrization available (acetonitrile). Altogether the nonelectronic interactions lead to a stabilization of the dimers with respect to the monomers (−1.5 kcal/mol). However, within the approach implemented in the GAUSSIAN program package the values computed for the different pairing modes of xanthine differ by less than 0.1 kcal/mol. Please note that computations for other solvents (nitromethane, water) lead to slightly different absolute values (between −1.0 and 2.0 kcal/mol), but also for these solvents the corrections do not differ for the various pairing modes. The small differences are expected since all pairing modes are quite similar in size and shape.

Employing the thermodynamic corrections obtained for the gas phase, we compute dimerization enthalpies between −3.3 and −5.1 kcal/mol (ΔH(gas) in Table 3, column 5) and positive dimerization free energies (ΔG(gas) in Table 4, column 2), i.e., in this approximation the computations fail to describe the pairing. Consequently, the influence of a polar medium on the thermodynamic corrections was evaluated. Initially, the TURBOMOLE program was used to estimate thermodynamic corrections in a polar solvent employing the COSMO approach ($\epsilon = 40$). While for the gas phase the sizes of the contributions leading to ΔG varied between 6.0 and 7.2 kcal/mol (ΔH: 0.7−1.4 kcal/mol), the values for a polar medium ranged from 6.1 to 6.4 kcal/mol, i.e., the effects became considerably more uniform.

By employing a continuum ansatz to estimate thermodynamic corrections, the influence of a polar solvent on the terms associated with vibrations (zero point energy contributions, ΔS_{vibr} etc.) is approximately taken into account; however, the translational entropies do not change since the gas-phase equations are used. For a rough estimate of the solvent effects on the translational entropy we employed a thermodynamic

TABLE 6: Computed and Measured ^{1}H NMR Chemical Shifts

	H1	H8	H3
5	12.14	7.33	6.46
7	11.36	7.34	6.60
8	11.61/11.71	7.35/7.38	6.54/6.44
Exp. (Xanthosine)	11.68/11.88	7.47	10.69

cycle proposed by Williams and co-workers.[28] In this approach the change in entropy when going from gas to a 1 M solution is broken down to a condensation to a pure liquid and to the subsequent dilution to a 1 M concentration. Transferring this approach to our problem the thermodynamic corrections leading to ΔG reduce to 3.9−4.2 kcal/mol and the dimerization free energies become negative (see Supporting Information). Please note, that this approach is not able to distinguish between different pairing modes.

Overall, our studies clearly show that the inclusion of the electrostatic interactions is most important for an understanding of the absolute and relative stabilities of the pairing modes. Other effects are more subtle but need to be considered for an analysis of absolute stabilities. Despite their small magnitudes they seem to be important for the relative stabilities of the pairing modes **5**, **7**, and **8**. Unlike **5** and **7**, dimer **8** can be formed in two different ways (unsymmetric pairing mode). Due to the influence on the entropy this effect will favor pairing mode **8** to some extent. However, since stability differences of the three pairing modes are only around 0.5 kcal/ mol at the present level, theory seems to be unable to predict the order of their stabilities. Please note that the uncertainties result not only from the description of solvent effects or thermodynamic corrections but are already associated with the underlying quantum chemical approaches (Table 1).

The inclusion of solvent effects leads to a better understanding of the magnitude of the various interactions; however, it still does not allow an unequivocal interpretation of the experimental data since differences between the experimentally accessible pairing modes **5**, **7**, and **8** are smaller than the error bars of the available theoretical methods. Therefore, NMR chemical shifts were computed for a more reliable interpretation of the experiments. Table 6 compares the computed ^{1}H NMR chemical shift values for the pairing modes **5**, **7**, and **8** with the experimental ones. A list of all computed values are summarized in the Supporting Information. The calculated spectrum for pairing mode **8** shows a very good agreement with the spectrum measured at 123 K. Calculated and experimental ^{1}H chemical shifts for the two H1 and the H8 hydrogen atoms differ by less than 0.2 ppm. Only the measured chemical shift for H3 of 10.69 ppm significantly differs from the computed chemical shifts of 6.54 and 6.44 ppm. This difference, however, can be attributed to the intramolecular hydrogen bond involving the ribosyl sugar moiety (see Figure 6), which is not included in the computed dimers. Overall, although the excellent agreement between theory and experiment seems to be somewhat fortuitous, the computations support the formation of pairing mode **8** for the xanthosine dimers.

In addition to the characterization of pairing geometries of xanthine, the experiment shows a considerably larger association constant for hypoxanthine dimers (200 ± 10 M^{-1}) compared to xanthine dimers (2.5 ± 0.3 M^{-1}). From the variation in the dimerization energies of the series **13** (−9.2 kcal mol^{-1}), **5** (−10.9 kcal mol^{-1}), **14** (−13.1 kcal mol^{-1}), and **12** (−14.4 kcal mol^{-1}), the hypoxanthine dimer **11** (Figure 8) is expected to possess a dimerization energy similar to **12** since it involves a C−X bond of little to no polarity. However, the dimerization

TABLE 7: Dimerization Energies of Hypoxanthine and 4,5-Dihydrohypoxanthine

	MP2/TZVPP $\epsilon = 1$	B3LYP/TZVPP $\epsilon = 1$	B3LYP/TZVPP $\epsilon = 40$	B3LYP/TZVPP $\epsilon = 78$
11	−18.7	−17.3	−5.1	−4.8
17	−14.0	−12.9		−3.3

energy of the noncanonical nucleobase hypoxanthine **11** is predicted to be −18.7 kcal/mol (MP2, Table 7), i.e., about 4 kcal/mol higher than expected.

This stabilization seems to be associated with the polarization of the π-electron system due to the hydrogen bond. For canonical base pairs, Guerra et al.[35] have shown that such effects result in a stabilization of −1 to −5 kcal/mol per hydrogen-bonded base pair. Furthermore, it has been demonstrated by Cyranski et al.[36] that the formation of hydrogen-bonded base pairs leads to an increase of the aromatic character of the nucleobases, in particular of guanine.

Figure 11 shows the relevant resonance structures. Structures **2b** and **2c** that correspond to an aromatic system are zwitterionic. The zwitterionic structures of **11** become somewhat more important upon dimerization, since the negative charge at the oxygen atom and the positive charge at the nitrogen atom can be delocalized through the hydrogen bonds of the dimer. As a consequence, the polarization of the π-electron system should play a more significant role for hypoxanthine dimer **11** than for the model systems **12**−**14** or the xanthine dimer **5**, for which the aromaticity is further disturbed by the additional functional groups. The aromatic contribution to the strength of hydrogen bonding can roughly be estimated by computing the dimerization energy for the model system **17** with a saturated C4═C5 double bond (Figure 12). For such a system the resonance structures **2b** and **2c** in Figure 11 no longer represent an aromatic situation.

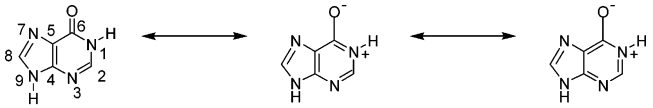

2a **2b** **2c**

Figure 11. Resonance structures of hypoxanthine.

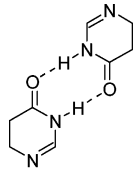

17

Figure 12. Dimer of model compound **17** which unlike hypoxanthine dimer **11** contains a saturated CC bond.

Indeed, the gas-phase dimerization energy of **17** is about 4.7 kcal/mol lower compared to the hypoxanthine dimer **11** (MP2), i.e., the aromaticity increases the hydrogen bond strength by about 2.3 kcal/mol per bond (Table 7). This difference in the dimerization energy is three times as large as the difference between pairing mode **5** of dixanthine and the model system **13**, where the polarization of the π-electron system cannot play such an important role. Their dimerization energies differ by 1.7 kcal/mol, i.e., 0.8 kcal/mol for each bond. Such effects also seem to be responsible for the differences in the dimerization energies computed for the uracil dimer **15** (−17.2 kcal/mol, Table 2) and the diamide **12** (−14.4 kcal/mol, Table 2). Similar dimerization energies have been obtained in the literature for the uracil dimer **15**.[37]

Secondary electrostatic effects which lead to large differences within the gas phase were largely eliminated in a polar

environment. Thus, the difference in the dimerization energy of **6** and **16** of 7.9 kcal/mol in the gas phase completely disappears for a very polar medium and the corresponding difference between **5** and **6** of 10.6 kcal/mol (B3LYP/TZVPP, Table 1) decreases to only 1.3 kcal/mol ($\Delta G(\epsilon = 40)$, Table 4). Stabilization effects arising from the polarization of the π-electron system seem to be less influenced. Going from the gas phase ($\epsilon = 1$) to water ($\epsilon = 78$), the difference between the hypoxanthine dimer **11** and the model system **17** decreases from 4.4 kcal/mol to 1.5 kcal/mol (Table 7). As a consequence its relative importance for hydrogen bonding is higher in a dielectric environment than in the gas phase. The reduced influence also explains, why **11** is less stable than **6** in the gas phase (−18.7 vs −22.0 kcal/mol) but becomes slightly more stable in a polar medium (−5.1 vs −4.8 kcal/mol).

The discussion about stabilities of xanthine dimers in polar solvents indicates that, in addition to electrostatic interactions, the nonelectronic interactions and the thermodynamic corrections are important for evaluating absolute stabilities. Employing the same approach as discussed for the xanthine dimers to obtain free dimerization energies in a polar solvent, we estimate a ΔG value of about −2.0 kcal/mol for the hypoxanthine dimer in a Freon matrix.[38] This value is about 1.4 kcal/mol more negative than the corresponding value of the xanthine dimer **8** which is expected to be formed based on the computations of the NMR chemical shifts. This trend nicely reflects the experimental data with considerably higher association constants for the hypoxanthine dimer ($2.5 \pm 0.3\ M^{-1}$ and $200 \pm 10\ M^{-1}$, respectively). According to our analysis, the difference between the stabilities of both dimers (**8** in comparison to **11**) mostly stems from the better polarization of the π-electron system within **11** (≈1.5 kcal/mol). Less repulsive secondary effects also contribute, but their importance is reduced within a polar medium (≈0.3 kcal/mol). Within our approach the thermodynamic corrections ($\Delta E \rightarrow \Delta G$) of both dimers estimated for a solvent is equal (3.9 kcal/mol).

Conclusions

In the present paper a combination of NMR experiments and quantum chemical calculations is used to characterize the abilities of xanthine and hypoxanthine in forming stable hydrogen-bonded dimers. While the NMR experiments on xanthosine and inosine are used to obtain accurate data about the stabilities of the formed complexes, the quantum chemical calculations of xanthine and hypoxanthine are employed to further interpret the experimental data and to more generally assess the relative stabilities of the various pairing modes and the interplay of the various effects on the stabilities.

A comparison of measured and calculated ^{1}H NMR chemical shifts show that xanthosine dimerizes in the pairing mode **8** (Figure 3, Table 6). Since the energy differences between the possible homodimers of xanthosine **5**, **7**, and **8** (Figure 3, Tables 1−2) are only around 0.5 kcal/mol at the present level, theory is not able to correctly describe their energetic order. The difference in the stability of formed xanthosine and inosine dimers is nicely described by our ansatz since the difference is larger than the expected error bars. Our computations also reliably show that other possible pairing modes **6**, **9**, and **10** of xanthine, which are not available in the xanthosine nucleoside, are expected to give more stable complexes (Figure 3, Tables 1−2).

The theoretical investigations also allow an insight into the interplay of the various effects that determine relative and absolute stabilities of the complexes. Since computations were performed for the gas phase as well as for a polar solvent, changes in the respective contributions due to the solvent were also accessible. In the gas phase the dimerization energies (ΔE) of the xanthine dimers range from those expected for normal two-dentate pairing modes (≈10−11 kcal/mol) to values indicating very strong hydrogen bonds (≈22 kcal/mol). Our analyses show that mainly secondary electrostatic effects are responsible for these large differences. The stability of the hypoxanthine dimer can be attributed to a favorable polarization of the π electron system that stabilizes the hydrogen bonds by about 5 kcal/mol (Table 7). Taking into account the influence of a polar solvent, the secondary electrostatic effects are largely abolished and the differences between the various pairing modes of xanthine decrease from about 10 kcal/mol in the gas phase to only about 1−2 kcal/mol in a polar medium. This change largely arises from the electrostatic contributions to the solvation energy. Also, the effect of polarizing the π electron system, which is important for the stability of the hypoxanthine dimer, is significantly weakened if the influence of the polar medium is taken into account (from about 5 kcal/mol in the gas phase to about 1.5 kcal/mol in a polar medium). However, the decrease is considerably smaller than the one found for the secondary electrostatic effects. As a consequence, the hypoxanthine dimer **11**, although less stable than pairing mode **6** of the xanthine dimer in the gas phase (B3LYP/TZVPP ($\epsilon = 1$): $\Delta E = -17.3$ vs −20.2 kcal/mol), becomes slightly more stable within a polar medium (B3LYP/TZVPP ($\epsilon = 40$): $\Delta E = -5.1$ vs −4.8 kcal/mol). All other effects, such as the so-called nonelectrostatic contributions to the solvation energy or thermodynamic contributions, are important for the absolute dimer stabilities but less important to understand their corresponding differences. Our analysis shows that the influence of the solvent on the thermodynamic corrections has to be taken into account for a correct description of the dimerization.

Acknowledgment. We thank U. Diederichsen for fruitful discussions. T.A.H. thanks the Fonds der Chemischen Industrie for a graduate scholarship. We thank the Deutsche Forschungsgemeinschaft for financial support within the framework of the project EN197/10 theoretical investigations to the molecular recognition of peptide nucleic acids. M.P.C. thanks the EU for a fellowship at the Marie-Curie Training site "Low Temperature Liquid and Solid State NMR-Spectroscopy of Hydrogen Transfer Systems" (HPTM-CT-2000-00127) at the Freie Universität Berlin.

Supporting Information Available: Absolute energies, counterpoise corrections, and Cartesian coordinates for the dimers **5**−**17** and the corresponding monomers. Additionally, thermodynamic corrections are given. This material is available free of charge via the Internet at http://pubs.acs.org.

References and Notes

(1) Kow, Y. W. *Free Radical Biol. Med.* **2002**, *33*, 886.

(2) Spence, J. P.; Jenner, J.; Chimel, K.; Aruoma, O. I.; Cross, C. E.; Wu, R.; Halliwell, B. *FEBS Lett.* **1995**, *375*, 179.

(3) The most stable isomer of xanthine is the N^7 regioisomer. It is about 7 kcal/mol more stable than the N^9 isomer, which is indicated in Figure 1. Xanthosine obtained from guanosine, however, only exists as in the N^9 form since for guanine (and the corresponding guanosine) the N^9 regioisomer represents the most stable form. Consequently, in the present study the bonding properties of N^9 regioisomers of xanthosine are characterized.

(4) Wink, D. A.; Kasprzak, K. S.; Maragos, C. M.; Elespuru, R. K.; Misra, M.; Dunams, T. M.; Cebula T. A.; Koch, W. H.; Andrews, A. W.; Allen, J. S. *Science* **1991**, *254*, 1001.

(5) Caulfeld, J. L.; Wishnok, J. S.; Tannenbaum, S. R. *J. Biol. Chem*. **1998**, *273*, 12689.
(6) Shapiro, R.; Pohl, S. *Biochemistry* **1968**, *7*, 448.
(7) Shapiro, R.; Shiuey, S. J. *Biochim. Biophys. Acta* **1969**, *174*, 403.
(8) Wuenschell, G. E.; O'Connor, T. R.; Termini, J. *Biochemistry* **2003**, *42*, 3608.
(9) Stoychev, G.; Kierdaszuk, B.; Shugar, D. *Eur. J. Biochem*. **2002**, *269*, 4048.
(10) Hernandez, B.; Luque, F. J.; Orozco, M. *J. Org. Chem*. **1996**, *61*, 5964. Hernandez, B.; Orozco, M.; Luque, F. J. *J. Comput.-Aided Mol. Design* **1996**, *10*, 535. Hoffmann, M. F. H.; Brückner, A. M.; Hupp, T.; Engels, B.; Diederichsen, U. *Helv. Chim. Acta*, **2000**, *83*, 2580. Rogstad, K. N.; Jang, Y. H.; Sowers, L. C.; Goddard, W. A., III *Chem. Res. Toxicol*. **2003**, *16*, 1455.
(11) Perrin, C. L.; Nielson, J. B. *Annu. Rev. Phys. Chem.* **1997**, *48*, 511. Hobza, P. *Annu. Rep. Prog. Chem., Sect. C: Phys. Chem.* **2004**, *100*, 3. Sponer, J.; Jurecka, P.; Hobza, P. *J. Am. Chem. Soc.* **2004**, *126*, 10142. Hobza, P.; Sponer, J. *J. Chem. Rev.* **1999**, *99*, 3247. Ojha, A. K.; Srivastava, S. K.; Koster, J.; Shukla, M. K.; Leszczynski, J.; Asthana, B. P.; Kiefer, W *J. Mol. Struct*. **2004**, *689*, 127.
(12) (a) Jorgensen, W. L.; Pranata, J. *J. Am. Chem. Soc.* **1990**, *112*, 2008. (b) Pranata, J.; Wierschke, S. G.; Jorgensen W. L. J. *Am. Chem. Soc.* **1991**, *113*, 2810. (c) Jorgensen, W. L.; Severance, D. L. *J. Am. Chem. Soc.* **1991**, *113*, 209.
(13) (a) Lukin, O.; Leszczynski, J. *J. Phys. Chem. A* **2002**, *106*, 6775. (b) Lukin, O.; Leszczynski, J. *J. Phys. Chem. A* **2003**, *107*, 9251.
(14) (a) Gilli, G.; Bellucci, F.; Ferretti, V.; Bertolasi, V. *J. Am. Chem. Soc.* **1989**, *111*, 1023. (b) Bertolasi, V.; Gilli, P.; Ferretti, V.; Gilli, G. *J. Am. Chem. Soc.* **1991**, *113*, 4917. (c) Gilli, P.; Bertolasi, V.; Ferretti, V.; Gilli, G. *J. Am. Chem. Soc.* **1994**, *116*, 909. (d) Bertolasi, V.; Gilli, P.; Ferretti, V.; Gilli, G. *Chem. Eur. J.* **1996**, *2*, 925. (e) Gilli, P.; Bertolasi, V.; Pretto, L.; Lyčka; Gastone, G. *J. Am. Chem. Soc*. **2002**, *124*, 13554.
(15) Golubev, N. S.; Smirnov, S. N.; Gindin V. A.; Denisov, G. S.; Benedict, H.; Limbach, H.-H. *J. Am. Chem. Soc.* **1994**, *116*, 12055.
(16) Ogilvie, K. K.; Thompson, E. A.; Quilliam, M. A.; Westmore, J. B. *Tetrahedron Lett.* **1974**, *33*, 2865.
(17) Dunger, A.; Limbach, H.-H.; Weisz, K. *J. Am. Chem. Soc.* **2000**, *122*, 10109.
(18) Becke, A. D. *J. Chem. Phys.* **1993**, *98*, 5648.
(19) Schäfer, A.; Huber, C.; Ahlrichs, R. *J. Chem. Phys.* **1994**, *100*, 5829.
(20) Boys, S. F.; Bernardi, F. *Mol. Phys.* **1970**, *19*, 553.
(21) Ahlrichs, R.; Bär, M.; Baron, H.-P.; Bauernschmitt, R.; Böcker, S.; Ehrig, M.; Eichkorn, K.; Elliott, S.; Furche, F.; Haase F.; Häser, M.; Horn, H.; Huber, C.; Huniar, U.; Kattaneck, M.; Kölmel, C.; Kollwitz, M.; May, K.; Ochsenfeld, C.; Öhm, H.; Schäfer, A.; Schneider, U.; Treutler, O.; Arnim, M.v.; Weigend, F.; Weis, P.; Weiss, H. *TURBOMOLE*, version 5.6; University of Karlsruhe, Germany, since 1988.
(22) Frisch, M. J.; Trucks, G. W.; Schlegel, H. B.; Scuseria, G. E.; Robb, M. A.; Cheeseman, J. R.; Zakrzewski, V. G.; Montgomery, J. A., Jr.; Stratmann, R. E.; Burant, J. C.; Dapprich, S.; Millam, J. M.; Daniels, A. D.; Kudin, K. N.; Strain, M. C.; Farkas, O.; Tomasi, J.; Barone, V.; Cossi, M.; Cammi, R.; Mennucci, B.; Pomelli, C.; Adamo, C.; Clifford, S.; Ochterski, J.; Petersson, G. A.; Ayala, P. Y.; Cui, Q.; Morokuma, K.; Malick, D. K.; Rabuck, A. D.; Raghavachari, K.; Foresman, J. B.; Cioslowski, J.; Ortiz, J. V.; Baboul, A. G.; Stefanov, B. B.; Liu, G.; Liashenko, A.; Piskorz, P.; Komaromi, I.; Gomperts, R.; Martin, R. L.; Fox, D. J.; Keith, T.; Al-Laham, M. A.; Peng, C. Y.; Nanayakkara, A.; Gonzalez, C.; Challacombe, M.; Gill, P. M. W.; Johnson, B.; Chen, W.; Wong, M. W.; Andres, J. L.; Gonzalez, C.; Head-Gordon, M.; Replogle, E. S.; Pople, J. A. *Gaussian 98*, revision A.7. Gaussian, Inc.: Pittsburgh, PA, 1998.
(23) Frisch, M. J.; Pople, J. A.; Binkley, J. S. *J. Chem. Phys*. **1984**, *80*, 3265.
(24) Schäfer, A.; Huber, C.; Ahlrichs, R. *J. Chem. Phys.* **1984**, *100*, 5829.
(25) Eichkorn, K.; Treutler, O.; Öhm, H.; Häser, M.; Ahlrichs, R. *J. Chem. Phys.* **1995**, *242*, 652.
(26) (a) Orozco, M.; Luque, F. J. *Chem. Rev.* **2000**, *100*, 4187. (b) Luque, J. F., Curutchet, C.; Munoz-Muriedas, J.; Bidon-Chanal, A.; Soteras, I.; Morreale, A.; Gelpi, J. L.; Orozco, M. *PhysChemChemPhys*, **2003**, *5*, 3827. (c) Cramer, C. J.; Truhlar, D. G. *Chem. Rev.* **1999**, *99*, 2161. (d) Orozco, M.; Colominas, C.; Luque, F. *J. Chem. Phys.* **1996**, *209*, 19. Curutchet, C.; Cramer, C. J.; Truhlar, D. G.; Ruiz-Lopez, M. F.; Rinaldi, D.; Orozco, M.; Luque, F. J. *J. Comput. Chem.* **2003**, *24*, 284.
(27) (a) Klamt, A.; Schürmann, G. J. *J. Chem. Soc., Perkin Trans*. **1993**, *2*, 799. (b) Schäfer, A.; Klamt, A.; Sattel, D.; Lohrenz, J. C. W.; Eckert, F. *PhysChemChemPhys* **2000**, *2*, 2187.
(28) Doig, A. J.; Williams, D. H. *J. Am. Chem. Soc.* **1992**, *114*, 338. Searly, M. S.; Williams, D. H. *J. Am. Chem. Soc.* **1992**, *114*, 10697.
(29) Häser, M.; Ahlrichs, R.; Baron, H. P.; Weis, P.; Horn, H. *Theor. Chim. Acta* **1992**, *85*, 455.
(30) Ochsenfeld, C. *Phys. Chem. Chem. Phys.* **2000**, *2*, 2153; Brown, S. P.; Schaller, T.; Seelbach, U. P.; Koziol, F.; Ochsenfeld, C.; Klarner, F.-G.; Spiess, H. W. *Angew. Chem., Int. Ed.* **2001**, *40*, 717.
(31) (a) Smirnov, S. N.; Golubev, N. S.; Denisov, G. S.; Benedict, H.; Schah-Mohammedi, P.; Limbach, H.-H. *J. Am. Chem. Soc.* **1996**, *118*, 4094. (b) Golubev, N. S.; Denisov, G. S.; Smirnov, S. N.; Shepkin, D. N.; Limbach, H.-H. *Z. Phys. Chem.* **1996**, *196*, 73. (c) Weisz, K.; Jähnchen, J.; Limbach, H.-H.; *J. Am. Chem. Soc*. **1997**, *119*, 6436. (d) Dunger, A.; Limbach, H.-H.; Weisz, K. *Chem. Eur. J*. **1998**, *4*, 621. (e) Basílio, J. E. M.; Dunger, A.; Limbach, H.-H.; Weisz, K.; *Magn. Reson. Chem*. **2001**, *39*, 177.
(32) Wüthrich, K. *NMR of Proteins and Nucleic Acids*; John Wiley & Sons: New York, 1986, pp 205−214.
(33) Smirnov, S. N.; Benedict, H.; Golubev, N. S.; Denisov, G. S.; Kreevoy, M. M.; Schowen, R. L.; Limbach, H.-H. *Can. J. Chem.* **1999**, *77*, 943.
(34) Corresponding CCSD(T) computations were not possible due to computational limitations.
(35) Guerra, C. F.; Bickelhaupt, F. M.; Snijders, J. G.; Baerends, E. J. *Chem. Eur. J.* **1999**, *5*, 3581.
(36) Cyranski, M. K.; Gilski, M.; Jaskolski M.; Krygowski, T. D. *J. Org. Chem* **2003**, *68*, 8607.
(37) Kratochvil, M.; Engkvist, O.; Sponer, J.; Jungwirth P.; Hobza, P. *J. Phys. Chem. A* **1998**, *102*, 6921.
(38) The size of the nonelectrostatic contributions is estimated to −1.15 kcal/mol (acetonitrile). The thermodynamic corrections to get from ΔE to ΔH (within a polar medium with $\epsilon = 40$) are 0.5 kcal/mol, while the influence of the entropy for $T = 128$ K ($\Delta H \rightarrow \Delta G$) is 3.4 kcal/mol. See Supporting Information for more information.